Discussion and Improvement of a Blade-Type XBPM with Coupling Suppression by Compensating Calibration Coefficients

J. Y. Chuang[1,2*], Y. Z. Lin[1*], Y. M. Hsiao[1], Y. C. Liu[1], D. Shu[3], C. K. Kuan[1], H. Wu[4], I. C. Sheng[5], Y. T Cheng[1], C. Shueh[1], C. C. Chang[1], C. K. Chan[1], J. Y. Yen[2]

1. National Synchrotron Radiation Research Center, 101 Hsin-Ann Road, Hsinchu Science Park, Hsinchu 30076, Taiwan, R.O.C.

2. Department of Mechanical Engineering, National Taiwan University, No. 1, Sec. 4, Roosevelt Road, Taipei, 10617 Taiwan, R.O.C.

3. Advanced Photon Source, Argonne National Laboratory, Argonne, IL 60439, USA

4. Department of Mechanical Engineering, University of Maryland, College Park, MD 20742, USA

5. Advanced Light Source, Lawrence Berkeley National Laboratory, Berkeley, CA 94720, USA

E-mail address: chuang.jy@nsrrc.org.tw (J.Y. Chuang), lin.yz@nsrrc.org.tw (Y.Z. Lin)

Corresponding author. Tel.: +886 3 5780281x6210, x6245

Total number of pages: 12

Total number of figures: 10

Total number of tables: 2

Abstract

The Taiwan Photon Source (TPS) is a third-generation, 3-GeV storage ring with a design current of 500 mA. To monitor the photon beam stability, blade-type X-ray beam position monitors (XBPMs) are installed to record and monitor the photon beam position. The beam position coordinates involve both the X- and Y-axes, and we must consider coupling effects in the XBPM, which have to be reduced for reliability and optimum precision. This study focuses on the front-end (FE) XBPM calibration via four-blade normalization and suppression matrix compensation. The calibration results show that in the optimal measurement range of $\pm$200 μm, the coupling effect between the X and Y position is suppressed to less than a 1-μm drift, which satisfies the high-accuracy beam position requirements for user operation. The reliability and precision of the XBPM system improved after applying the serial calibration process developed in this study, and the detailed derivation of each calibration step will be discussed in this paper.

Keywords: blade-type XBPM, coupling effect, suppression matrix

1. Introduction

Blade-type X-ray beam position monitors (XBPMs) in BL front-ends (FEs) are essentially detectors of beam position in synchrotron radiation facilities [1-3]. With an XBPM, we can obtain an accurate beam position measurement after careful calibration. G. Decker pointed out in 1999 that stray radiation affects the accuracy of XBPMs. Therefore, the use of XBPMs is improved by, for example, changing the lattice to eliminate light contamination from upstream bending magnets [4]. In 2011, V.P. Dhamgye used electron asymmetric bump control for the Indus-2 XBPM system to perform calibration studies. The goal was to observe Cu-blade signals as they were displaced to obtain consistent signals after adjusting the calibration factors [5]. Many studies have shown that before using an XBPM as an indicator for beam stability, a reliable calibration process must be completed before feeding the signal into a feedback system to stabilize the beam position. Due to its advantages, the photoemission blade-type XBPM is widely used in synchrotron radiation facilities, and it is becoming a standard diagnostic component for noninvasive position monitoring and orbit feedback [6].

Most studies use difference over sum equations to calculate the beam position [7, 8] of XBPMs. These equations are based on linear equations to determine the beam position using four-blade signals. However, few studies have discussed the coupling effect and blade normalization method. Some considerations, such as different coating qualities of each blade, beam profile, beam motion direction and spatial assembly tolerances (as shown in Fig. 1), could affect the sensitivities of the XBPM blades. Case I in Fig. 1 is an ideal symmetric assembly, while other cases show possible issues induced by mechanical assembly tolerances, which, according to our assembly experience, are 50 to 100 μm. Due to these issues, the XBPM calibration method must consider center alignment, blade normalization, position scaling and offset compensation.

To improve the traditional position calculation, we regard the XBPM system as a quadrant detector (QD) system because both systems are designed with the same four-quadrant sensors and same position determination method. For a QD system, all the calibration coefficients are usually determined through a calibration method that uses a light source with a known profile to fit the measured signals and compensate for the sensors [9, 11]. However, this method is difficult to realize in a synchrotron radiation facility because of the high-energy beam and the need to prevent encroachment on the beam. Therefore, this study proposes a calibration method that determines a series of calibration coefficients such that the TPS XBPM can decouple efficiently and perform with high precision and reliability after calibration.

2. Construction of the XBPM system

2.1 Diamond blades

A photoemission-type diamond blade is an efficient device for beam diagnostics that can withstand the high heat load and dose rate that occur in third-generation synchrotron radiation facilities operating at 500 mA [12]. A 100-μm-thick chemical vapor deposition (CVD)-fabricated diamond detector, coated with thin films of 0.1 μm Ti, 0.12 μm Pt and 0.3 μm Au, is used to emit a photo-current that can

be used to determine the beam position. Each blade is connected to a BNC-type feedthrough via a Kapton wire, and the blade pitches are 5 mm (horizontal) and 3 mm (vertical) (Fig. 2).

2.2 Data acquisition and scanning control system

The design of the XBPM scanning control system is based on the Libera Photon system, which is used data acquisition (DAQ) and analog to digital converter (ADC) for the photoemission currents measurement. Each blade is connected to a standard noise rejection cable, 30 m in length, via a coaxial BNC-type feedthrough to transmit the signals to the Libera Photon system. The DAQ parameters are compiled in Table 1 [13]. We integrated translation stage control and the data recording system to scan the XBPM system for calibration.

The XBPM scanning control system consists of a stage with 1-μm precision driven by a 1:100 harmonic stepper motor and feedback via both a 1000-count encoder and a potentiometer. Depending on the high-precision design and assembly, the translation stages before the online operation were inspected to verify that the coupling errors along both the X and Y axes were less than 2 μm.

3. Signal processing and calibration method

3.1 Fundamental theory of XBPM signal processing

To determine the beam position in a horizontal (X) and vertical (Y) coordinate system by solving the difference over sum equations, as given by Eqs. 1 and 2, which use the blade photoemission currents:

$$X = K_x \frac{(V^A - V^B - V^C + V^D)}{(V^A + V^B + V^C + V^D)} = K_x \frac{\Delta x}{\sum x} \quad (1)$$

$$Y = K_y \frac{(V^A + V^B - V^C - V^D)}{(V^A + V^B + V^C + V^D)} = K_y \frac{\Delta y}{\sum y} \quad (2)$$

where

X and Y are the positions of the photon beam,

K_x and K_y are corrected coefficients,

V^A,V^B,V^C, and V^D are the photoemission currents from the respective diamond blades,

Δx and Δy are the differences in the current of two pairs of blades (in the X-axis scanning are AD and BC, and in the Y-axis scanning are AB and CD), and

$\sum x$ and $\sum y$ are the sums of photoemission current in the four blades.

Considering the blade normalization, a built-in formula (3) of the Libera Photon system [13], which is a 4-by-4 matrix, must be employed to compensate for the variations between the photoemission currents of each blade, thereby improving the accuracy of the XBPM system and removing coupling issues.

$$\begin{bmatrix} \Delta x \\ \Sigma x \\ \Delta y \\ \Sigma y \end{bmatrix} = \begin{bmatrix} a_{0x} & b_{0x} & c_{0x} & d_{0x} \\ a_{1x} & b_{1x} & c_{1x} & d_{1x} \\ a_{0y} & b_{0y} & c_{0y} & d_{0y} \\ a_{1y} & b_{1y} & c_{1y} & d_{1y} \end{bmatrix} \begin{bmatrix} V^A \\ V^B \\ V^C \\ V^D \end{bmatrix} \quad (3)$$

where

$\begin{bmatrix} a_{0x} & b_{0x} & c_{0x} & d_{0x} \\ a_{1x} & b_{1x} & c_{1x} & d_{1x} \\ a_{0y} & b_{0y} & c_{0y} & d_{0y} \\ a_{1y} & b_{1y} & c_{1y} & d_{1y} \end{bmatrix}$ is a 4-by-4 matrix for the four-blade normalization and

$\begin{bmatrix} V^A \\ V^B \\ V^C \\ V^D \end{bmatrix}$ is a 1-by-4 matrix for the four-blade input photoemission currents.

3.2 Derivation of beam position calculation

Using the difference over sum equations, we obtain the displacement (X, Y) by satisfying two conditions. First, the variation of the blade signals and XY displacements must be linear. Second, the sum of blade currents (Σx and Σy) during the scanning must be approximately constant. To meet these two conditions for the blade-type XBPM system used in this study, the system must pass steps (a) to (c) to stay within certain measurement and linear conditions for photon beam displacement (X, Y). For explicit discussions, an FE TPS41A elliptically polarizing undulator (EPU) source with the gap 24 mm and horizontal linear mode polarization is used as an example for calibration.

(a) Blade function determination

Due to the numerators and denominators of Eqs. 1 and 2 are general algebraic expressions, which means the blade behavior in the linear condition is necessary. We can establish Eq. 4 as the axial equation for the diamond blades after linear fitting. Figure 3 shows the X- and Y axes scanning result

for four blades in the range of ± 1 mm. Using the Y-axis scanning as an example to derive steps (a) to (c).

$$V^A = m_y^A \mathrm{y} \quad A \rightarrow B, C, D \tag{4}$$

where

m_y^A is the blade sensitivity slope, the superscript is the blade name, the subscript is the scanning axis, and y is the stage position with 100 μm per step.

(b) Sum of the four-blade photoemission currents is a constant

From the dotted line in Fig. 3 Y-axis scanning position, which represents the sum of the four-blade photoemission current, the tolerance of ±15 μA is small and can be considered as constant. Therefore, we can assume the denominator Σx and Σy of Eqs. 1 and 2 is a constant.

(c) According to the experimental verification in the previous two steps, a final Eq. 5 is derived as shown below (using the Y-axis position as an example):

$$\begin{aligned} Y &= K_y \frac{\Delta y}{\sum y} - y_0 \\ &= K_y \frac{(V^A + V^B - V^C - V^D)}{V^A + V^B + V^C + V^D} - y_0 = K_y \frac{(m_y^A y + m_y^B y - m_y^C y - m_y^D y)}{\sum y} - y_0 \\ &= K_y \frac{\bar{m} y}{\sum y} - y_0 = \frac{K_y}{\sum y} (\bar{m} y) - y_0 \end{aligned} \tag{5}$$

where

$$\bar{m} = m_y^A + m_y^B - m_y^C - m_y^D \tag{6}$$

$$\Sigma y = V^A + V^B + V^C + V^D \tag{7}$$

and the intercept y_0 is used as the offset to simplify the calculation.

Experimental results and the derivation of the three steps (a), (b) and (c) are shown in Fig. 4. After analyzing the XBPM measurement results in the Y-axis scanning, the residual sum of squares (RSS) is 1.06×10^{-6}, which, from a linear fit perspective, suggests a highly linear behavior and proves that Eq. 5 is a linear equation, indicating that the XBPM is aligned in the center region of the photon beam. These

steps also apply to the X-axis position calculation, with the signs and subscripts for each blade being changed to *x*.

3.3 Determination of the calibration coefficients

When measuring any physical quantity, its sensors include a region that can be approximated by a linear equation. We use linear fitting to determine the linear region of the diamond blade with a blade sensitivity slope (m_x^i, m_y^i) as shown in Eq. 4. Depending on the different scanning directions and some background issues, as shown in Fig. 5, m_x^i and m_y^i can be defined individually. Then, a sensitivity slope of one arbitrarily chosen diamond blade is taken as the reference for the relative gain sensitivity *G* compared with other blades, which can lead to inconsistencies between G_x^i and G_y^i by X- and Y-axis scanning.

Let B, C, and D be the blades compared with a reference A. The gain sensitivities G_x^i and G_y^i of the respective blades are obtained using Eqs. 8 and 9 for the X and Y directions:

$$G_x^i = \frac{m_x^A}{m_x^i} \qquad i \to B, C, D \tag{8}$$

$$G_y^i = \frac{m_y^A}{m_y^i} \qquad i \to B, C, D \tag{9}$$

The XBPM is a physical system that measures a synchrotron beam intensity as an input, and the beam position (X and Y) as an output by calculating. The output position (X, Y) with the blade normalization effectiveness is obtained by multiplying the gain sensitivities G_x^i and G_y^i by the input of the blade signals. In the signal processing flow, G_x^i and G_y^i are cascaded in the flow and can be merged into N^i by multiplication, and we named the total gain sensitivity as shown in Eq. 10. Thus, the total gain sensitivities of *B*, *C*, and *D* blades consist of gain sensitivities along both the X- and Y-axis, and the new blade function is obtained as Eq. 11 after normalize the sensitivities of each blade. The calibration coefficients are compiled in Table 2.

Since blade A is the reference, N^A=1, and

$$N^i = G_x^i G_y^i \quad i \to B, C, D \tag{10}$$

$$V^{A'} = N^A V^A = N^A m_y^A \mathrm{y} = N^A m_x^A x \quad A \to B, C, D \tag{11}$$

where $V^{A'}$ is the new blade function after normalization.

Consequently, using $\frac{1}{G_x^i}$ and $\frac{1}{G_y^i}$ in the matrix, we can isolate the total gain sensitivities of the two axes into a matrix called the suppression matrix. Specifically, for the XY projected plane, we correct the displacement components along the Y-axis as we scan along the X-axis by multiplying the G_y^i , and vice versa. After substitution, Eq. 3 becomes Eq. 12:

$$\begin{bmatrix}\Delta x\\ \Sigma x\\ \Delta y\\ \Sigma y\end{bmatrix}=\begin{bmatrix}a_{0x} & b_{0x} & c_{0x} & d_{0x}\\ a_{1x} & b_{1x} & c_{1x} & d_{1x}\\ a_{0y} & b_{0y} & c_{0y} & d_{0y}\\ a_{1y} & b_{1y} & c_{1y} & d_{1y}\end{bmatrix}\begin{bmatrix}N^A & 0 & 0 & 0\\ 0 & N^B & 0 & 0\\ 0 & 0 & N^C & 0\\ 0 & 0 & 0 & N^D\end{bmatrix}\begin{bmatrix}V^A\\ V^B\\ V^C\\ V^D\end{bmatrix}=\begin{bmatrix}1 & \frac{-1}{G_x^B} & \frac{-1}{G_x^C} & \frac{1}{G_x^D}\\ 1 & \frac{1}{G_x^B} & \frac{1}{G_x^C} & \frac{1}{G_x^D}\\ 1 & \frac{1}{G_y^B} & \frac{-1}{G_y^C} & \frac{-1}{G_y^D}\\ 1 & \frac{1}{G_y^B} & \frac{1}{G_y^C} & \frac{1}{G_y^D}\end{bmatrix}\begin{bmatrix}V^{A'}\\ V^{B'}\\ V^{C'}\\ V^{D'}\end{bmatrix} \quad (12)$$

To scale the standard scanning stroke of $\pm$ 1 mm by $\frac{\Delta x}{\sum x}$ and $\frac{\Delta y}{\sum y}$, corrected coefficients *Kx* and *Ky* can be obtained. After averaging the offset positions for the X and Y axes, we obtain x_0 and y_0. The final *X* and *Y* positions are then defined by Eqs. 13 and 14, respectively.

$$X = K_x \frac{\Delta x}{\sum x} - x_0 \quad (13)$$

$$Y = K_y \frac{\Delta y}{\sum y} - y_0 \quad (14)$$

Figure 6 shows the signal processing flow of the overall calibration process. All coefficients, gain sensitivities (G_x^i and G_y^i), total gain sensitivities (N^i), suppression matrices, and corrected coefficients (K_x, K_y) are utilized in each step of the calibration process.

4. Calibration results

To practice the calibration method developed in this study, an ideal XBPM system must independently provide X and Y positions without coupling after calibration. For example, when the photon beam moves along the X-axis, there should be no drifting errors from coupling effects along the Y-axis. To compare the decoupling performance before and after calibration, the XBPM can be observed to be within $\pm$ 1 mm, and the slope of stationary axis drifting improves from X = 0.0782, Y =

0.1289 to X=0.0035, Y=0.0045, as shown in Figs. 7 and 8. To discuss the measurement precision, for the center range within ±200 μm with a minimum drifting error, the root mean squares are X=0.7 μm and Y=0.8 μm, and the resolution can be determined as 1 μm along both the X- and Y-axes, which is sufficient to monitor the beam position in most beam-time operations.

The 2D matrix scans shown in Fig. 9 and 10 illustrate the results of the range +/- 2 mm measurement performance before and after calibration for comparison. The distortion of XBPM position has been eliminated after calibration, and this result proves that the calibration process of XBPM in this study has practical applicability.

5. Conclusions

The arguments presented in this paper are based on calibration results for specific parameters such as ID gap or polarization mode, and the measurement performance has been verified for the calibration process by compensating the gain sensitivities and suppression matrix. This calibration process behaves similarly in both the 41A (EPU) and 23A (in-vacuum undulator, IU) FEs, confirming the correctness of the calibration process in the TPS. Due to all calibration coefficients of the diamond blades being determined via numerical calculation and blade characteristic quantification, the calibration process can be programmed in an automatic calibration system for a large synchrotron radiation facility. This system could help simplify the calibration and maintain the XBPM for high-precision measurements based on the calibration process developed in this study.

Acknowledgments

We would like to thank National Taiwan University NSRRC Precision Mechanical Group, Instrument Control Group, and especially our colleagues who contributed to the mechanical design, vacuum system construction, signal acquisition system and FE installation.

References

[1] Huang, C. H., Wu, C. Y., Chiu, P. C., Cheng, Y. S., Liao, C. Y., Hu, K. H., & Hsu, K. T. (2019, January). X-ray beam position monitors and their usage at the Taiwan photon source. In AIP Conference Proceedings (Vol. 2054, No. 1, p. 060053). AIP Publishing.

[2] Shu, D., Rodricks, B., Barraza, J., Sanchez, T., & Kuzay, T. M. (1992). The APS X-ray undulator photon beam position monitor and tests at CHESS and NSLS. *Nuclear Instruments and Methods in Physics Research Section A: Accelerators, Spectrometers, Detectors and Associated Equipment*, *319*(1-3), 56-62.

[3] Aoyagi, H., Kudo, T., & Kitamura, H. (2001). Blade-type X-ray beam position monitors for SPring-8 undulator beamlines. *Nuclear Instruments and Methods in Physics Research Section A: Accelerators, Spectrometers, Detectors and Associated Equipment*, *467*, 252-255.

[4] Decker, G., Singh, O., Friedsam, H., Jones, J., Ramanathan, M., & Shu, D. (1999). Reduction of X-BPM systematic errors by modification of lattice in the APS storage ring. In *Proceedings of the 1999 Particle Accelerator Conference (Cat. No. 99CH36366)*(Vol. 3, pp. 2051-2053). IEEE.

[5] Dhamgaye, V. P., Lodha, G. S., & Kane, S. R. (2011). Beam position measurements of Indus-2 using X-Ray beam position monitor. Nuclear Instruments and Methods in Physics Research Section A: Accelerators, Spectrometers, Detectors and Associated Equipment, 659(1), 525-527.

[6] T Kim, C., Shin, S., Hwang, I., Lee, B. J., Joo, Y. D., Ha, T., ... & Kim, I. (2015). Correlation study of a beam-position monitor and a photon-beam-position monitor in the PLS-II. Journal of the Korean Physical Society, 66(2), 167-170.

[7] Hubert, N., Béchu, N., Dasilvacastro, J., Cassinari, L., Denard, J. C., Labat, M., ... & Neuenschwander, R. (2014). Design of a new blade type X-BPM.WEPD22, IBIC, CA, USA.

[8] Keane, R., Bui, H., Decker, G., Hahne, M., Wimmer, C., & Leban, P. EVALUATION OF A VARIETY OF PHOTON BEAM POSITION MONITOR DATA ACQUISITION METHODOLOGIES AT THE APS.

[9] Narag, J., & Hermosa, N. (2017). Response of quadrant detectors to structured beams via convolution integrals. JOSA A, 34(7), 1212-1216.

[10] Li, Q., Wu, J., Chen, Y., Wang, J., Gao, S., & Wu, Z. (2018). High Precision Position Measurement Method for Laguerre-Gaussian Beams Using a Quadrant Detector. Sensors, 18(11), 4007.

[11] Zhao, T., Li, B., Li, C., Wang, R., Miao, Q., Liang, K., ... & Han, D. (2017). New distortion correction algorithm for two-dimensional tetra-lateral position-sensitive silicon photomultiplier. IEEE Electron Device Letters, 38(2), 228-231.

[12] Shu, D., Kuan, C. K., Sheng, I. C., & Chen, J. R. (2013). Development of an x-ray beam position monitor for TPS EPU beamline front ends. In Journal of Physics: Conference Series (Vol. 425, No. 4, p. 042003). IOP Publishing.

[13] Libera Photon. (2016). Photon Beam Position Monitor user Manual and Specifications.

Note: This table is established by taking blade A as a standard comparison with the gain sensitivity of blades B, C, and D (i = B, C, D).

Fig 1.

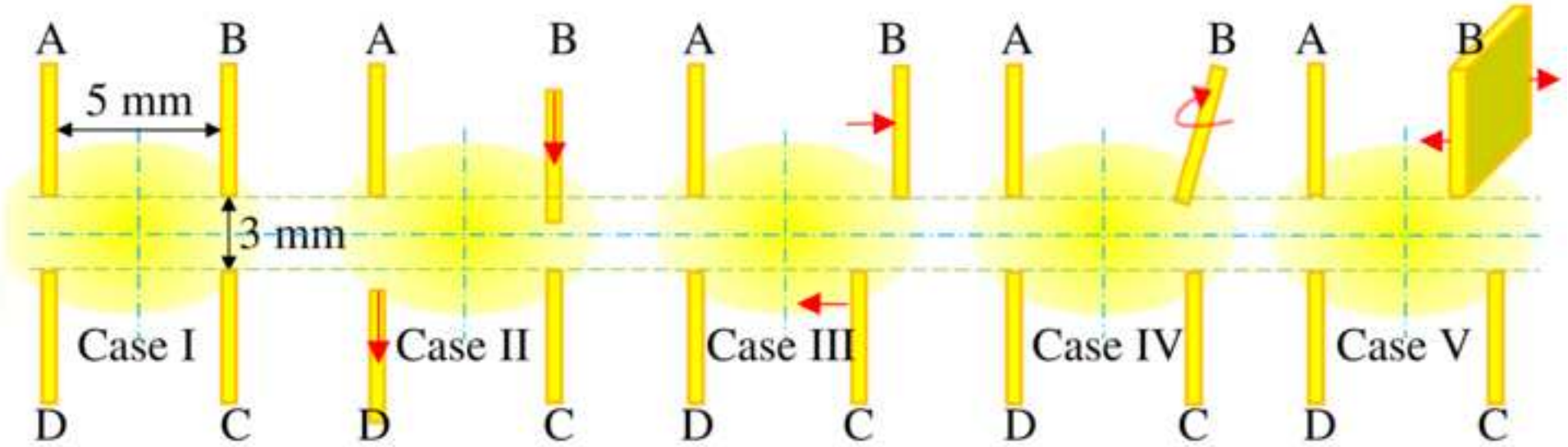
A
B
A
B
A
B
A
B
A
B
5 mm
3 mm
Case I
Case II
Case III
Case IV
Case V
D
C
D
C
D
C
D
C
D
C

Fig 2.

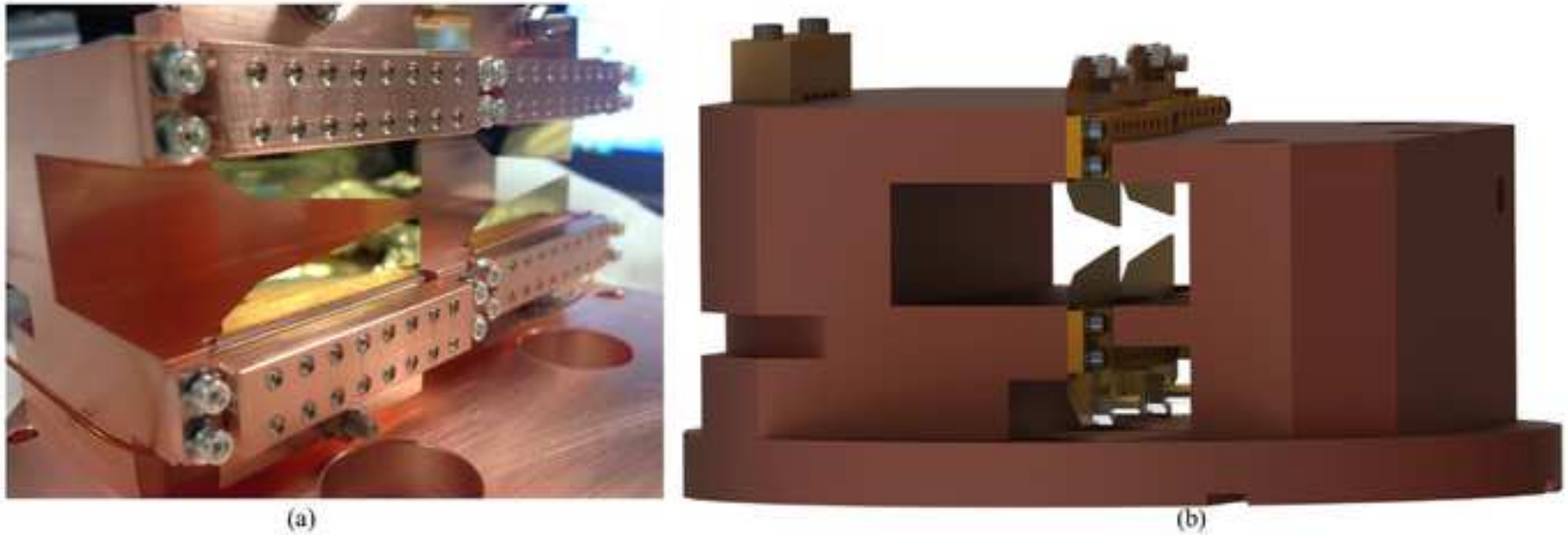

(a) (b)

Fig 3.

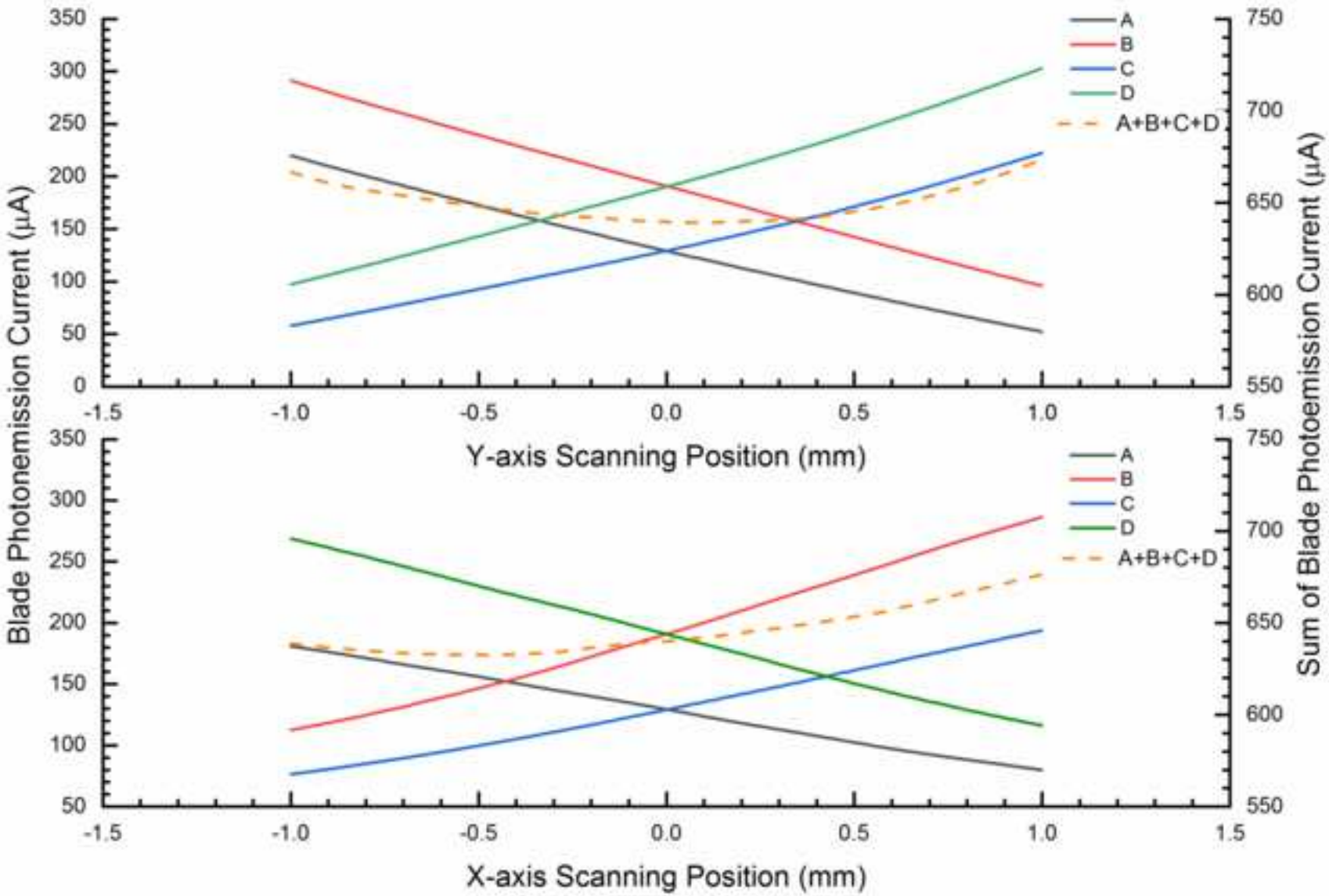
Blade Photonemission Current (μA)
Sum of Blade Photoemission Current (μA)
Y-axis Scanning Position (mm)
X-axis Scanning Position (mm)
A
B
C
D
A+B+C+D
350
300
250
200
150
100
50
0
750
700
650
600
550
-1.5
-1.0
-0.5
0.0
0.5
1.0
1.5

Fig 4.

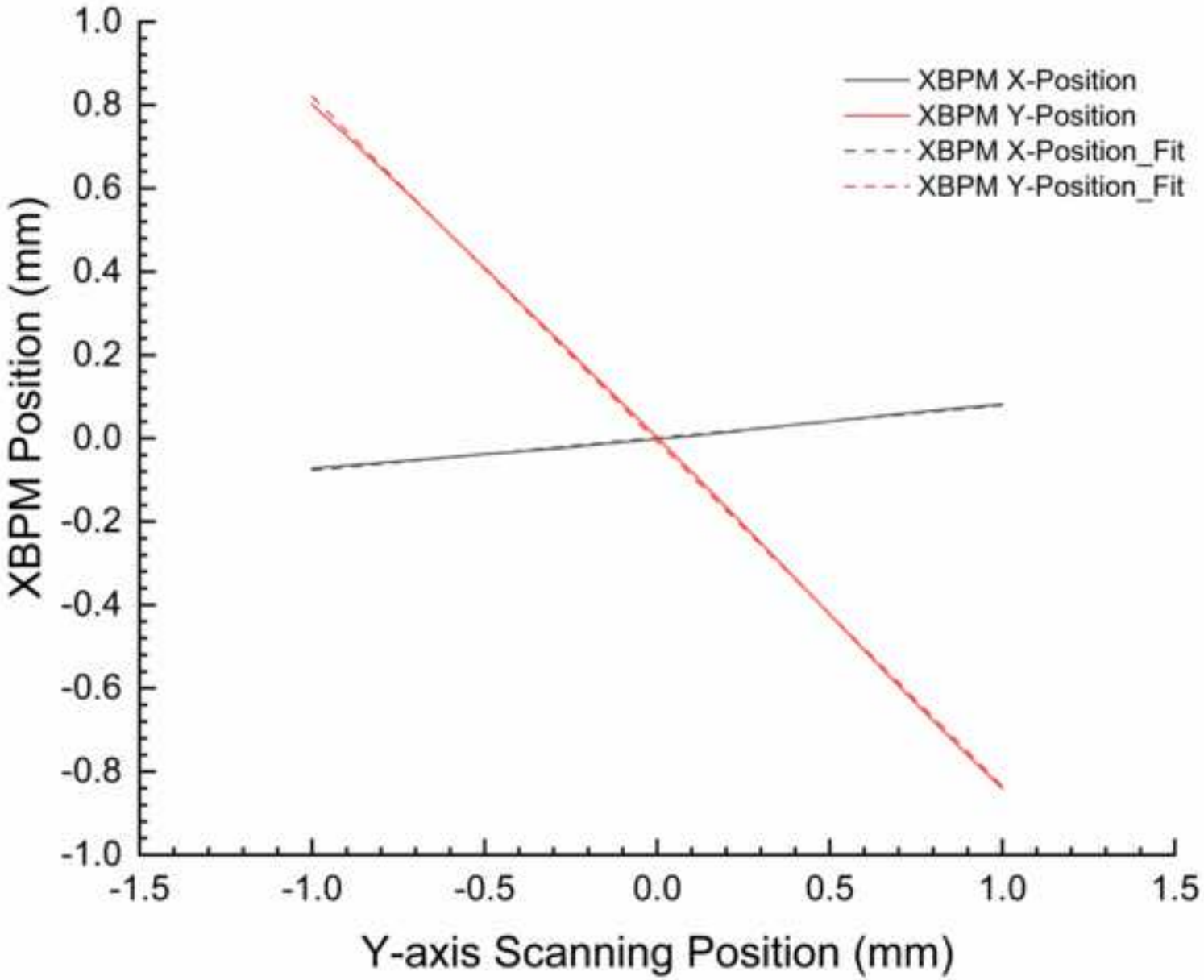
XBPM X-Position
XBPM Y-Position
XBPM X-Position_Fit
XBPM Y-Position_Fit
XBPM Position (mm)
Y-axis Scanning Position (mm)
1.0
0.8
0.6
0.4
0.2
0.0
-0.2
-0.4
-0.6
-0.8
-1.0
-1.5
-1.0
-0.5
0.0
0.5
1.0
1.5

Fig 5.

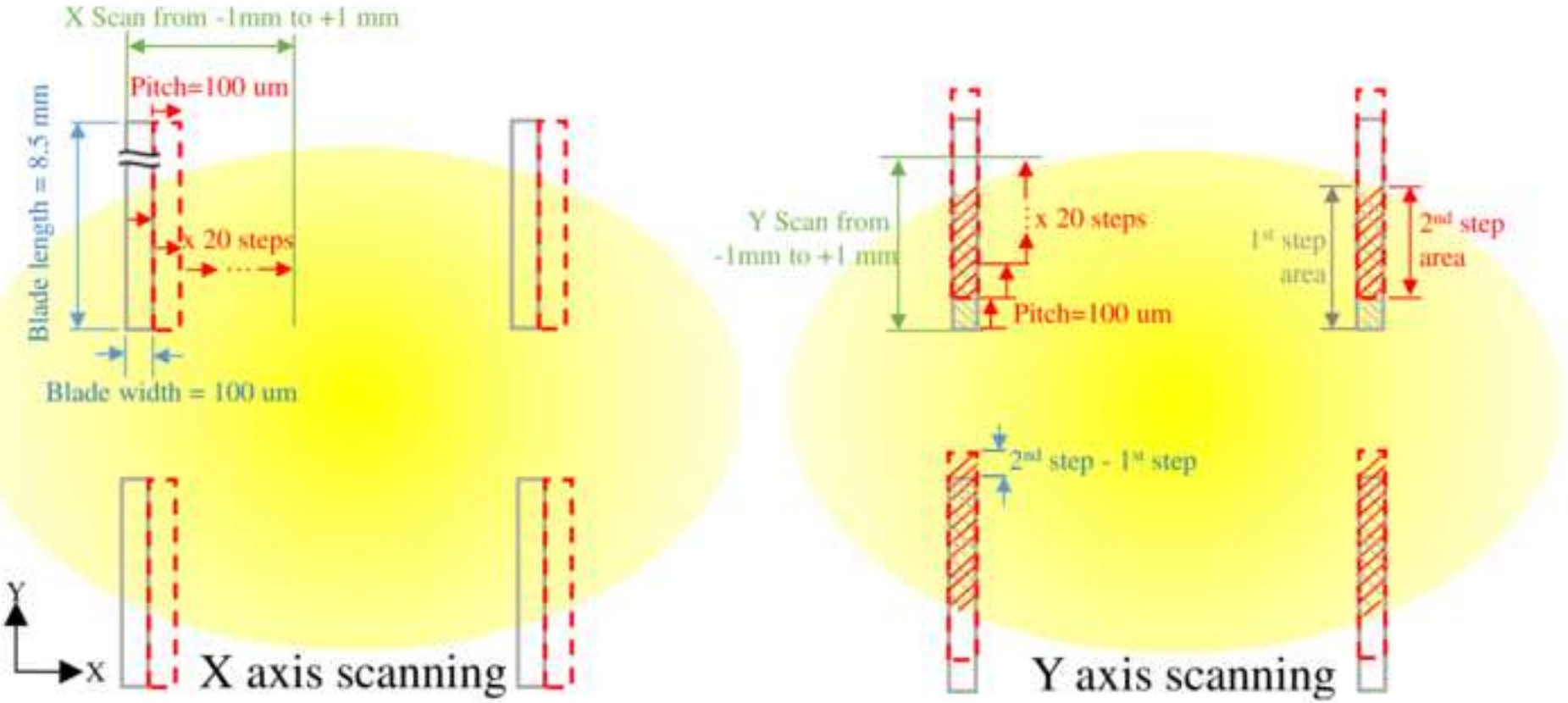
X Scan from -1mm to +1 mm
Pitch=100 um
Blade length = 8.5 mm
x 20 steps
Blade width = 100 um
Y
X
X axis scanning
Y Scan from
-1mm to +1 mm
x 20 steps
Pitch=100 um
1st step
area
2nd step
area
2nd step - 1st step
Y axis scanning

Fig 6.

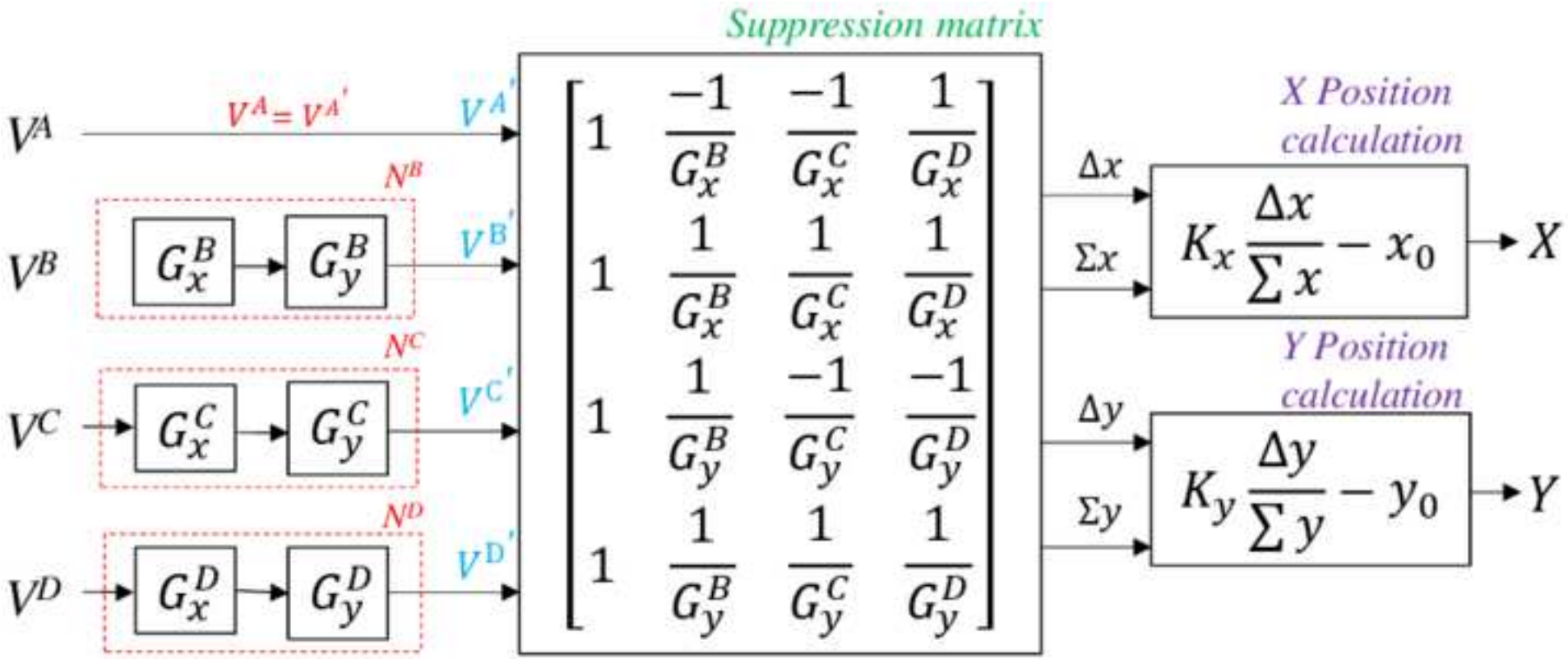
Suppression matrix
X Position calculation
Y Position calculation
V^A
V^B
V^C
V^D
$V^A = V^{A'}$
N^B
N^C
N^D
$V^{A'}$
$V^{B'}$
$V^{C'}$
$V^{D'}$
G_x^B
G_y^B
G_x^C
G_y^C
G_x^D
G_y^D
$\begin{bmatrix} 1 & \frac{-1}{G_x^B} & \frac{-1}{G_x^C} & \frac{1}{G_x^D} \\ 1 & \frac{1}{G_x^B} & \frac{1}{G_x^C} & \frac{1}{G_x^D} \\ 1 & \frac{1}{G_y^B} & \frac{-1}{G_y^C} & \frac{-1}{G_y^D} \\ 1 & \frac{1}{G_y^B} & \frac{1}{G_y^C} & \frac{1}{G_y^D} \end{bmatrix}$
Δx
Σx
Δy
Σy
$K_x \frac{\Delta x}{\sum x} - x_0$
$K_y \frac{\Delta y}{\sum y} - y_0$
X
Y

Fig 7.

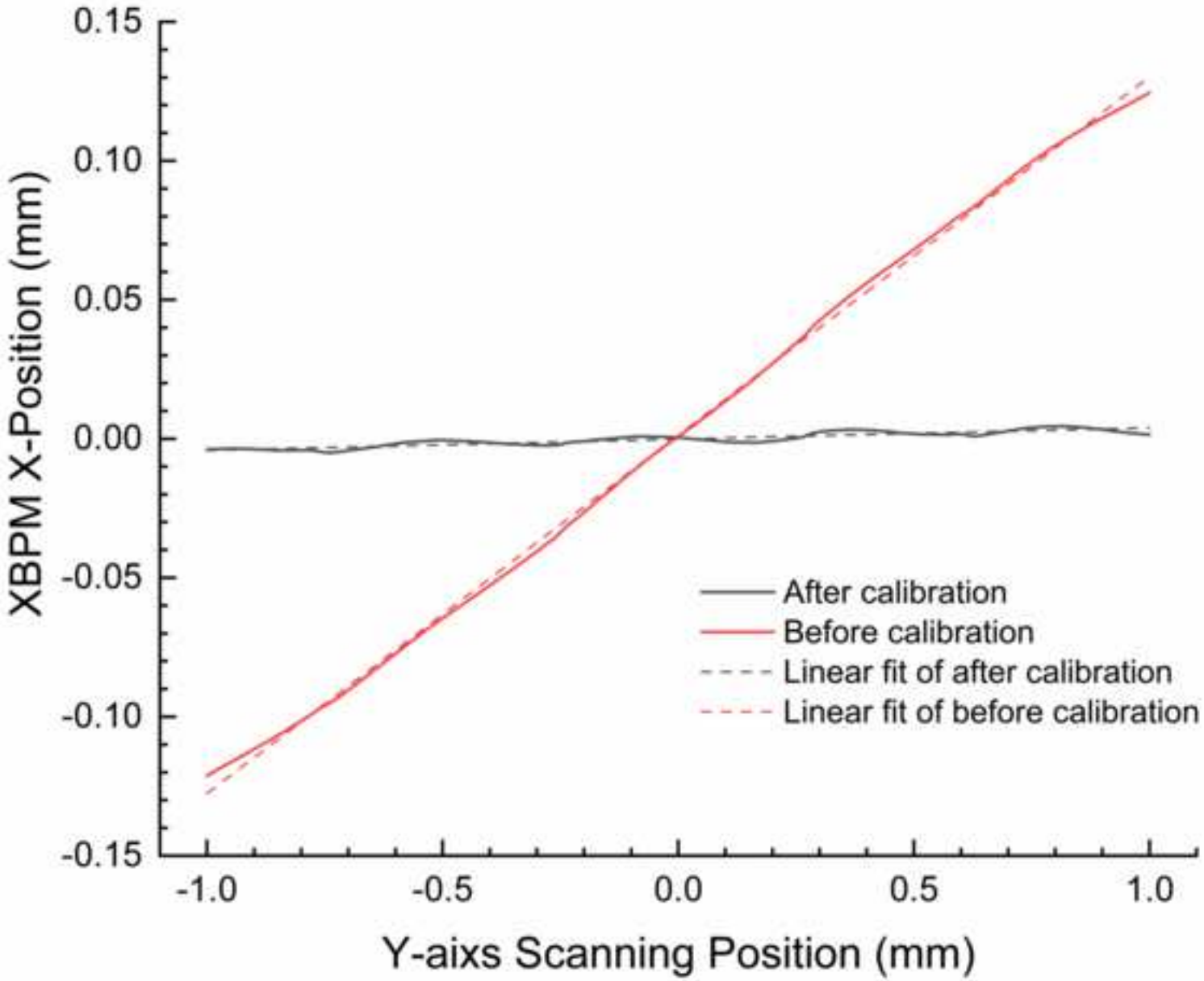
0.15
0.10
0.05
0.00
-0.05
-0.10
-0.15
XBPM X-Position (mm)
-1.0
-0.5
0.0
0.5
1.0
Y-aixs Scanning Position (mm)
After calibration
Before calibration
Linear fit of after calibration
Linear fit of before calibration

Fig 8.

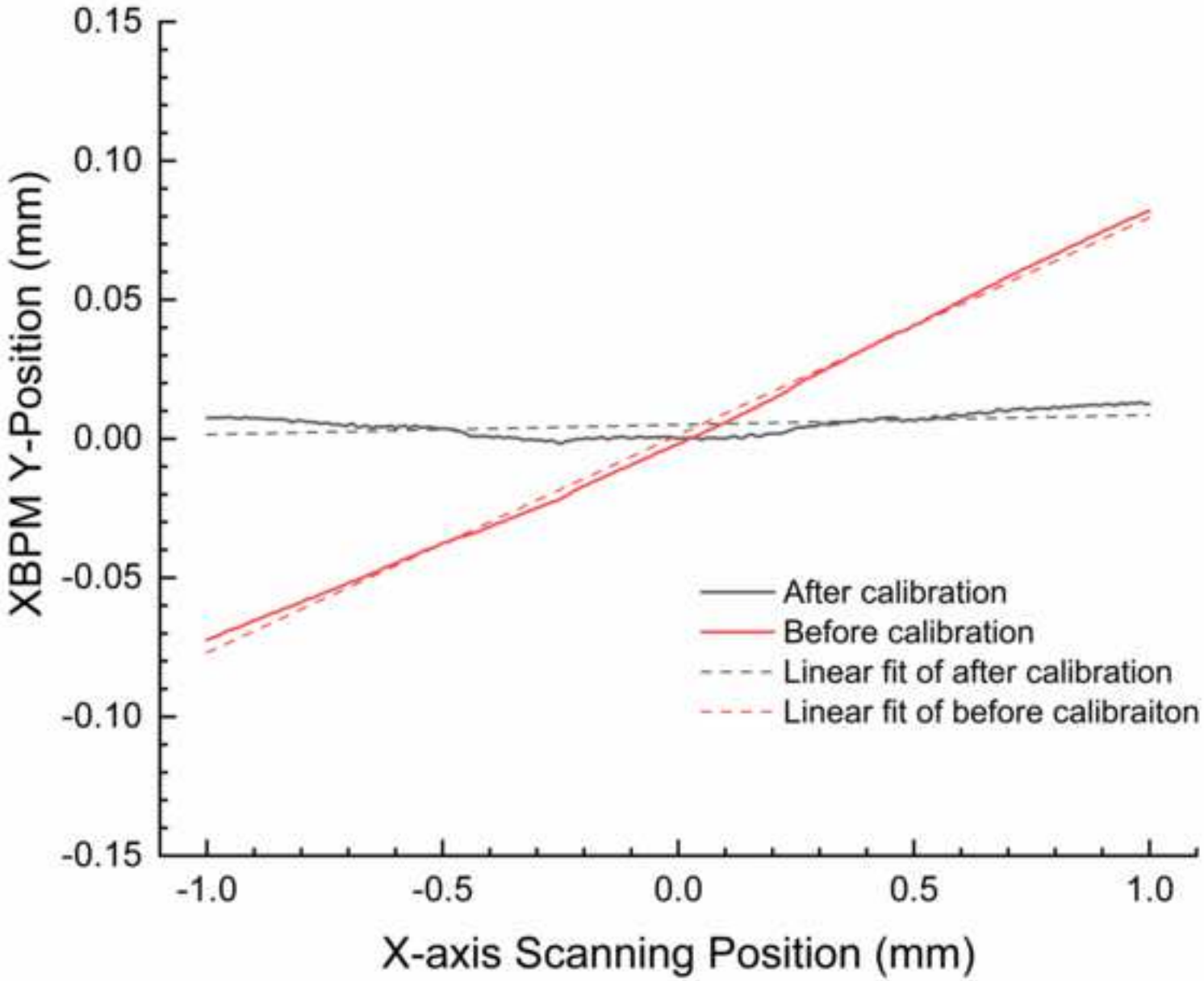
0.15
0.10
0.05
0.00
-0.05
-0.10
-0.15
XBPM Y-Position (mm)
-1.0
-0.5
0.0
0.5
1.0
X-axis Scanning Position (mm)
After calibration
Before calibration
Linear fit of after calibration
Linear fit of before calibraiton

Fig 9.

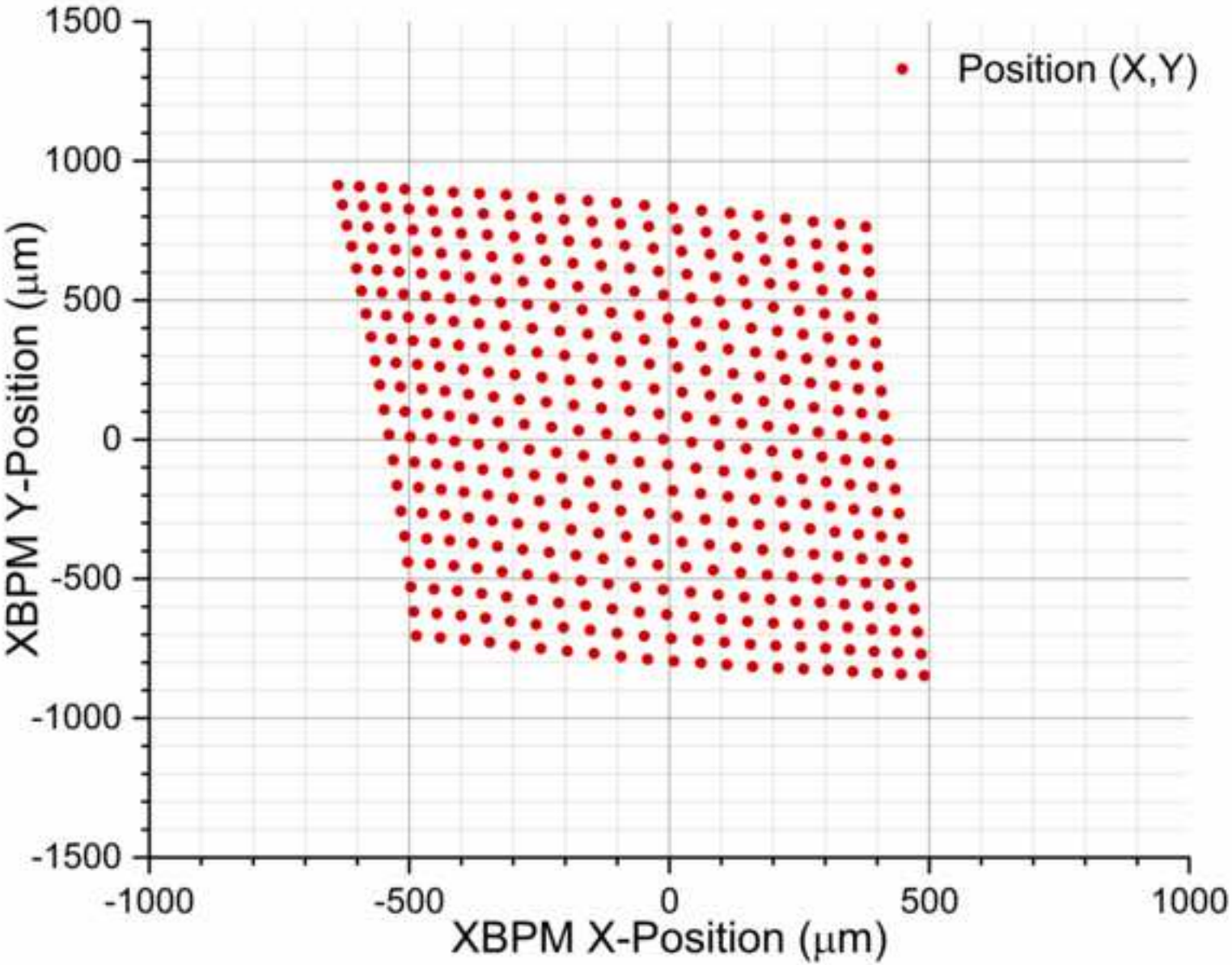
Position (X,Y)
XBPM Y-Position (μm)
XBPM X-Position (μm)
1500
1000
500
0
-500
-1000
-1500
-1000
-500
0
500
1000

Fig 10.

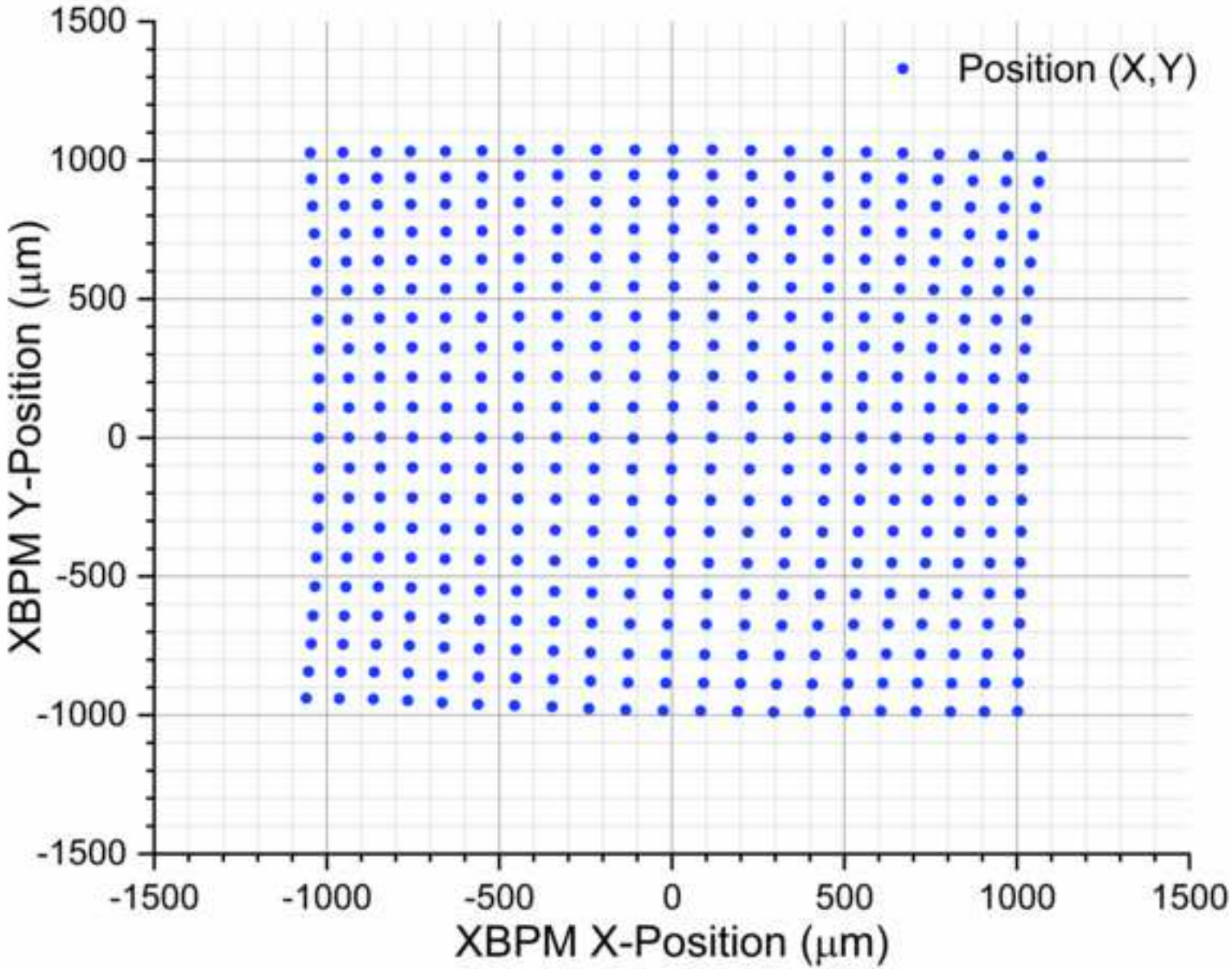
Position (X,Y)
1500
1000
500
0
-500
-1000
-1500
XBPM Y-Position (μm)
-1500
-1000
-500
0
500
1000
1500
XBPM X-Position (μm)

Table 2

	m_x	m_y	$G_x^i = \left\lvert \frac{m_x^A}{m_x^i} \right\rvert$	$G_y^i = \left\lvert \frac{m_y^A}{m_y^i} \right\rvert$	$N^i = G_x^i G_y^i$
A	-52.07	-83.68	1	1	1
B	89.94	-97.36	0.58	0.86	0.50
C	60.13	80.52	0.87	1.04	0.90
D	-78.12	101.13	0.67	0.83	0.55

Note: This table is established by taking blade A as a standard comparison with the gain sensitivity of blades B,

Table 1

ADC converter	18-bit
A/D sampling clock	2-2.5 MHz
Nominal range	+/- 2 mA
Slow acquisition (SA)data rate	25 Samples/sec
Amplifier bandwidth	>40 kHz